J Mater Sci (2011) 46:4675–4682
DOI 10.1007/s10853-011-5374-2

Phase diagram and electric properties of the (Mn, K)-modified $Bi_{0.5}Na_{0.5}TiO_3$–$BaTiO_3$ lead-free ceramics

Min Xu · Feifei Wang · Tao Wang · Xinman Chen · Yanxue Tang · Wangzhou Shi

Received: 15 October 2010 / Accepted: 7 February 2011 / Published online: 18 February 2011

Abstract In this study, the phase diagram and electric properties were demonstrated for a (Mn, K)-modified $Bi_{0.5}Na_{0.5}TiO_3$ (BNT)-based solid solution. $(0.935-x)\,Bi_{0.5}Na_{0.5}TiO_3-xBi_{0.5}K_{0.5}TiO_3-0.065BaTiO_3$ with 0.5% mol Mn doping was prepared by a conventional solid-state reaction method. A morphotropic phase boundary (MPB) formed between the ferroelectric rhombohedral and tetragonal phases around x of 0.04 with the MPB tolerance factor t of 0.984–0.986. The temperature and composition dependence of the dielectric, piezoelectric, ferroelectric properties along with the strain characteristics were investigated in detail and a phase diagram was presented. Around the MPB region, the maximum values of piezoelectric constant d_{33}^* of 290 pC/N, d_{33} of 155 pC/N, dielectric constant $\varepsilon_{33}^T/\varepsilon_0$ of 1059 and low dielectric loss tangent tan δ of 0.017 were obtained. In addition, the authors also suggest that the solid solution with composition x of 0.24, exhibiting both high-depolarization temperature T_d of 182 °C, d_{33}^* of 156 pC/N, d_{33} of 130 pC/N, will be favorable for high-temperature actuator and sensor applications.

Introduction

Piezoelectric materials play an important role in electromechanical devices such as sensors, actuators, and ultrasonic transducers. Most piezoelectric devices are designed and fabricated with traditional $Pb(Zr,Ti)O_3$ (PZT)-based piezoelectric ceramics because of their excellent piezoelectric and electromechanical properties [1]. However, owing to the environmental concerns over their lead oxide toxicity, environmental legislation in the European Union, parts of Asia, and the US demands elimination of toxic lead for these materials systems [2] and this spurred a large effort in the research of new piezoelectric lead-free materials in the past few years [3–9].

Among them, $Bi_{0.5}Na_{0.5}TiO_3$ (BNT)-based family is one of the promising lead-free systems and it was first discovered by Smolenskii et al. in 1961 [10]. Owing to its high-coercive field and electrical conductivity, pure BNT ceramic is hard to be poled completely to achieve desired piezoelectric and dielectric response [10]. Therefore, extensive BNT-based systems especially with the composition around the morphotropic phase boundary (MPB) region have been developed such as $Bi_{0.5}Na_{0.5}TiO_3$–$BaTiO_3$ (BNT–BT) [11], $Bi_{0.5}Na_{0.5}TiO_3$–$Bi_{0.5}K_{0.5}TiO_3$ (BNT–BKT) [12], $Bi_{0.5}Na_{0.5}TiO_3$–$SrTiO_3$ (BNT–ST) [13] etc., and the piezoelectric properties along with the electrical resistivity have been greatly improved. Recently, Ren and Liu [14] reported another exciting lead-free system of $Ba(Ti_{0.8}Zr_{0.2})O_3$–$(Ba_{0.7}Ca_{0.3})TiO_3$ (BTZ–BCT), indicating ultrahigh piezoelectric constant d_{33} of $\sim$620 pC/N, entirely comparable to the traditional PZT systems. Nevertheless, these new systems suffer some common problems, especially the strong-temperature dependence of obtainable electric-field-induced strain. Take the BTZ-BCT for example, the working temperature is limited to below 70 °C [14] and this greatly restricts the practical application prospective. Therefore, some ternary solid solutions such as $Bi_{0.5}Na_{0.5}TiO_3$–$Bi_{0.5}Li_{0.5}TiO_3$–$Bi_{0.5}K_{0.5}TiO_3$ (BNT–BLT–BKT) [15], $Bi_{0.5}Na_{0.5}TiO_3$–$Bi_{0.5}K_{0.5}TiO_3$–$BaTiO_3$ (BNT–BKT–BT) [16] have been proposed to further improve its piezoelectric response along with the depolarization and Curie temperature.

M. Xu · F. Wang (✉) · T. Wang · X. Chen · Y. Tang · W. Shi
Key Laboratory of Optoelectronic Material and Device, Mathematics & Science College, Shanghai Normal University, Shanghai 200234, China
e-mail: f_f_w@sohu.com

Among them, the BNT–BKT–BT system attracted much attention because of both high piezoelectric response and depolarization/Curie temperature compared with other BNT-based solid solutions such as BNT–BT or BNT–BKT [11, 12, 16]. However, so far about this system the temperature-induced phase transition characteristics along with the frequency dispersion behavior have been seldom reported. The relationship between the phase diagram, tolerance factor t and the MPB composition, and the systematic electric properties in BNT–BKT–BT system are also desired. Therefore, it is quite necessary for us to clarify these relations for promoting its applications to solid-state actuators and transducers.

On the other hand, relatively high dielectric loss for the BNT-based solid solution remains an important issue to be resolved. It has been demonstrated that introducing additives into the solid solution is one effective way is to further adjust the microstructure. In this study, the phase transition, frequency dispersion behavior along with the dielectric, ferroelectric, and piezoelectric properties were investigated in detail for the BNT–BKT–BT solution. A 0.5% mol Mn ion was simultaneously doped as an additive which has been verified able to create a "hard" effect so as to reduce the dielectric loss [17, 18]. The relationship between the phase diagram and the electrical properties was demonstrated. Besides, the tolerance factor t dependence of the MPB composition was also discussed. The maximum values of piezoelectric constant d_{33}^* of 290 pC/N, d_{33} of 155 pC/N, $\varepsilon_{33}^T/\varepsilon_0$ of 1059 and low loss tangent tan δ of 0.017 were obtained around the MPB region.

Experimental

$(0.935-x)Bi_{0.5}Na_{0.5}TiO_3$-$xBi_{0.5}K_{0.5}TiO_3-0.065BaTiO_3-0.005Mn$ (BNKBMTx, $x = 0$, 0.04, 0.08, 0.12, 0.16, 0.20, 0.24, and 0.28) ceramics were prepared by a conventional solid-state reaction method using Bi_2O_3 (99.0%), Na_2CO_3 (99.8%), K_2CO_3 (99.0%), $BaCO_3$ (99.0%), TiO_2 (98.0%), and MnO_2 (97.5%) as starting raw materials. For each composition, the starting materials were weighed according to the stoichiometric formula and ball-milled for 6 h in ethanol. The dried slurries were calcined at 850 °C for 2 h and then ball-milled again for 6 h. The powders were subsequently pressed into green disks with a diameter of 15 mm under 4 MPa. Using a heating rate of 3 °C/min, sintering was carried out at 1170–1250 °C for 2 h in covered alumina crucibles. To minimize the evaporation of the volatile elements Bi and Na, the disks were embedded in a powder of the same composition. Silver paste was coated on both sides of the sintered samples and fired at 650 °C for 0.5 h to form electrodes. The specimens for measurement of piezoelectric properties were poled in silicone oil bath with a dc field of 4–5 kV/mm at 70–80 °C for 15 min. All the electrical measurements were performed after aging for at least 24 h.

The crystal structures of the sintered ceramics were characterized by X-ray diffractometry (D8 Focus, Germany). Dielectric constant and loss of the ceramics were measured using an automatic acquisition system with an impedance analyzer (Agilent HP4294A,) in the temperature range of 25–400 °C. The d_{33} values of the poled samples were measured using a Berlincourt d_{33} meter at 55 Hz. P-E loops and S-E curves, where P, E, and S denote the polarization, the electric field and the strain, respectively, were measured under an electric field of 4 kV/mm in silicon oil with the aid of a Sawyer–Tower circuit.

Results and discussion

Phase structure analysis

Figure 1a–c shows the X-ray diffraction (XRD) patterns of the fabricated BNKBMTx ceramics with x from 0 to 0.28. Here the powder diffraction file (PDF) of $BaTiO_3$ from JCPDS is also shown in Fig. 1d for reference. From Fig. 1a and c, the patterns indicate that all compositions were crystallized into a single-phase perovskite structure and no trace of second phase existed. In order to give an insight into the room temperature phase, the 2θ range of 38.5°–41.5° and 45°–48°, corresponding to the (111) and (200) diffraction peaks, are illustrated in Fig. 1b and c. It is generally known that the difference between rhombohedral and tetragonal phases in the perovskite materials can be easily distinguished by the {111} and {200} profiles of XRD patterns. The rhombohedral phase is characterized by the splitting of the (111) and $(\bar{1}11)$peaks while the tetragonal one is characterized by the splitting of the (200) and (002) peaks. From Fig. 1b and c, it is evident that for x smaller than 0.04, the rhombohedra is the dominant phase while with x further increasing to above 0.08, the crystal lattice was distorted and become the tetragonal one. The ceramics with x around 0.04–0.08 locate around MPB, exhibiting the coexistence of ferroelectric rhombohedral and tetragonal phases. Based on the relationship between the composition and the tolerance factors t $\left(t = (R_A + R_O)/\sqrt{2}(R_B + R_O)\right)$ proposed in related study [19], the MPB tolerance factor t_{MPB} of the proposed ternary solution can be calculated to be 0.984 for x of 0.04 and 0.986 for x of 0.08 using Shannon's ionic radii [20], which locate around the MPB region and coincide with the experience value of t_{MPB} (0.982–0.986) very well [19]. Besides, obvious peak shifting behavior with K

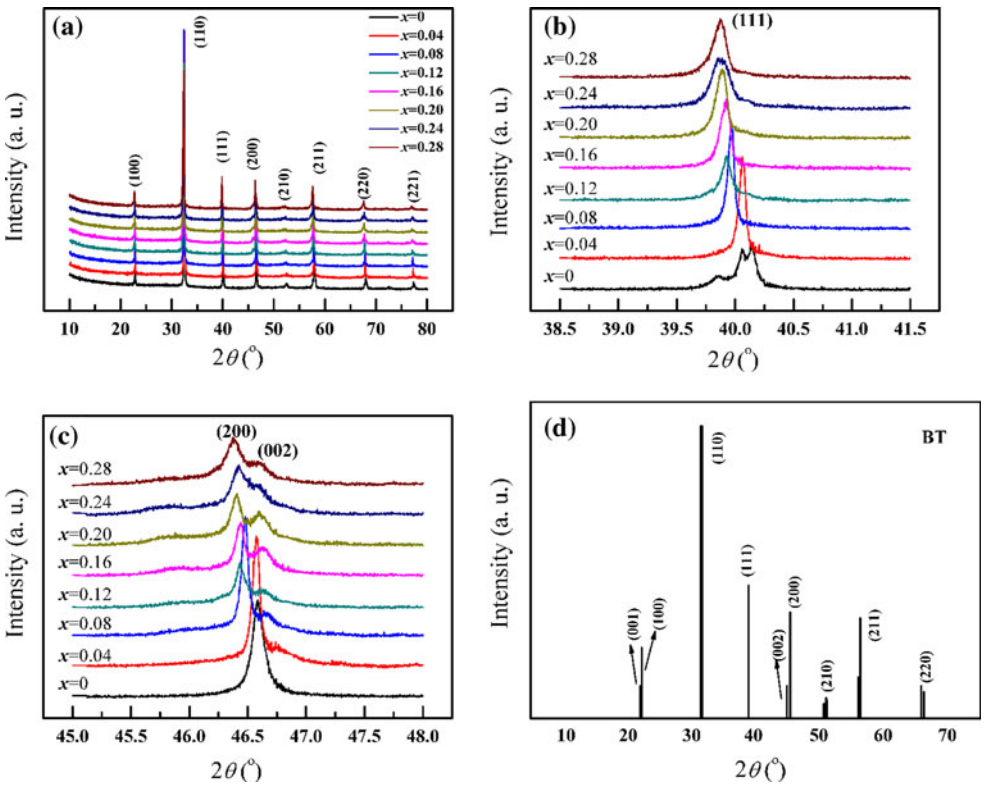

Fig. 1 X-ray diffraction patterns of the BNKBMTx ceramics with pure perovskite structure, **a** XRD pattern with the 2θ range of 10°–80°, **b** the (111) peak with the 2θ range of 38.5°–41.5°, **c** the (200)/(002) peak with the 2θ range of 45°–48°, and **d** the standard power diffraction file of the tetragonal $BaTiO_3$ from the JCPDS

concentration increasing can be observed from Fig. 1b and c because of the larger ionic radius of K^+ than Na^+.

Dielectric properties

Figure 2a–h illustrates the composition and temperature dependence of the dielectric constant $\left(\varepsilon_{33}^T/\varepsilon_0\right)$ and loss (tanδ) from 25 to 400 °C with the x of 0–0.28 under the frequency of 100 Hz to 100 kHz. From all the figures, two dielectric anomalies can be observed, which corresponds to the dielectric-maximum temperature (T_m) and the depolarization temperature (T_d), respectively, as summarized in Fig. 3. Around the T_m, broad dielectric peaks can be observed for all the compositions, exhibiting diffuse phase transition characteristics. This is correlated with the multiple complexes in the A-site (such as Bi^{3+}, Na^{1+}, Ba^{2+}, K^+, etc.) of perovskite compounds, which could lead to the compositional inhomogeneity in nanoscale [21]. The depolarization temperature T_d, determined from the peaks of the dielectric loss, is another important factor for BNT-based lead-free ceramics in view of their practical application. For x below 0.04, the T_d corresponds to the ferroelectric rhombohedral to antiferroelectric phase transition temperature and for x above 0.08 it is related to the ferroelectric tetragonal to pseudocubic (tetragonal) phase transition temperature based on the analysis of BNT–BKT [12] and the XRD results. For the ferroelectric phases below T_d, weak frequency dispersion behavior can be well-observed from the dielectric spectrum Fig. 2a–h. This indicate that in the poled ceramics, the macrodomain was dominant and the motion of these macrodomains could be fast enough to follow the external applied electric field, leading to the weak frequency dispersion. However, when the temperature increases over T_d, the ferroelectric order would be disrupted because of the ferroelectric phase transition, accompanied with the greatly enhanced frequency dispersion behavior.

From Figs. 2 and 3, it can be observed that the T_m increases quasi-linearly from 240 to 291 °C and the maximum dielectric constant first increases with the K content increasing (0–0.08) and then follow a decreasing with higher K content (0.08–0.28). In comparison, the T_d first shifts to lower temperature for x below 0.04, then follow an increase for x over 0.08. Around the MPB region between the ferroelectric rhombohedral and tetragonal phases, the T_d reaches the minimum value of 82 °C because of the phase coexistence as shown in Fig. 3.

Figure 4 shows the composition dependence of the $\varepsilon_{33}^T/\varepsilon_0$ and tanδ of samples before and after poled under 1 kHz at room temperature. For the unpoled ceramics, the $\varepsilon_{33}^T/\varepsilon_0$ decreases from 1,515 to 1,218 with the K

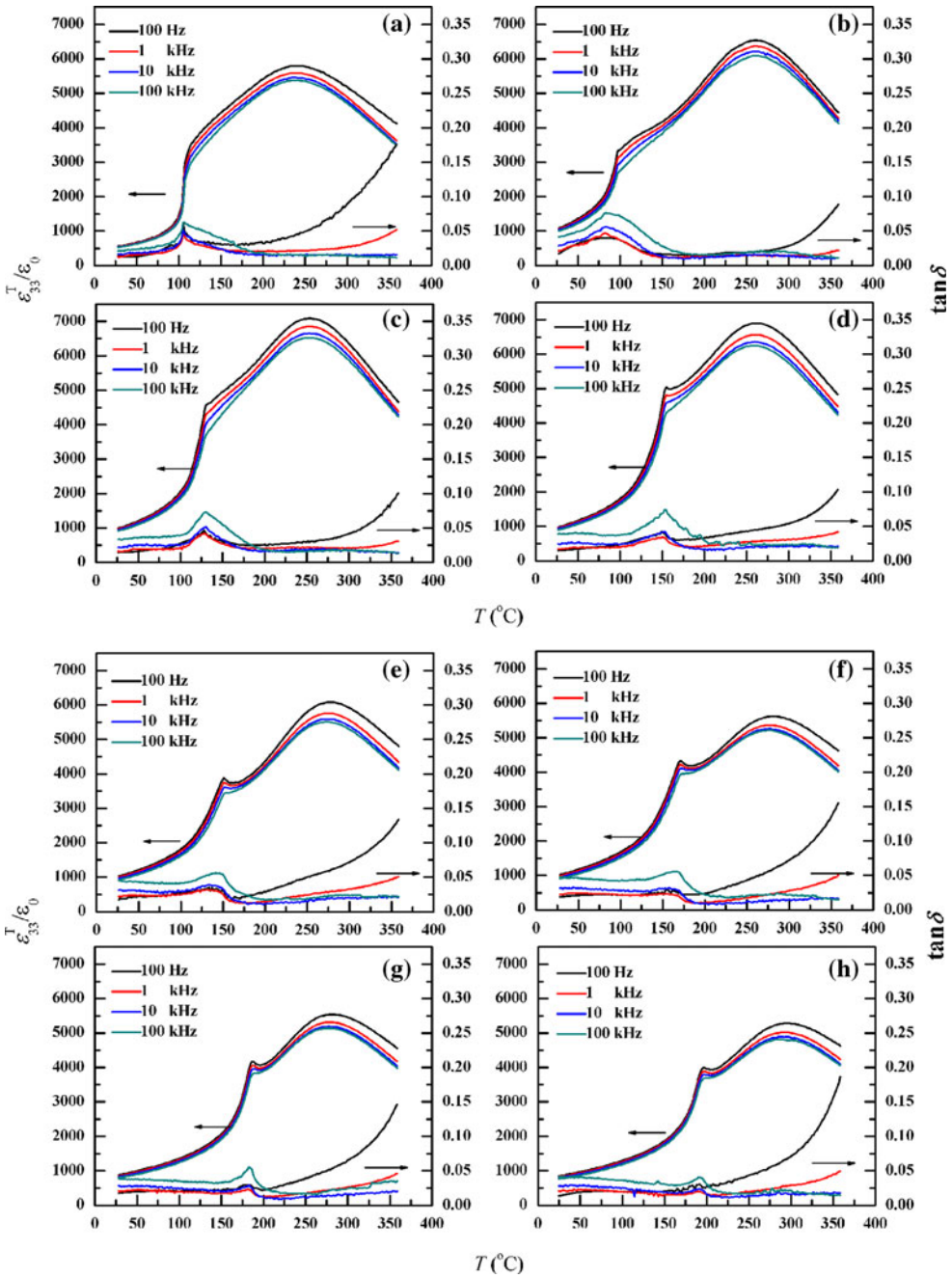

Fig. 2 Frequency, composition and temperature dependence of the relative dielectric constant $\varepsilon_{33}^T/\varepsilon_0$ and dielectric loss tanδ from 25 to 400 °C under the frequency of 100 Hz–100 kHz with the composition x, **a** 0, **b** 0.04, **c** 0.08, **d** 0.12, **e** 0.16, **f** 0.20, **g** 0.24, and **h** 0.28

concentration increasing while the tanδ increases from 0.027 to 0.042. After poled, the electrical dipoles were aligned along the external field direction and the $\varepsilon_{33}^T/\varepsilon_0$and tan$\delta$ both decreased greatly because of the reduced domain mobility, ranging from 700 to 1,059 and 0.015 to 0.022. The maximum $\varepsilon_{33}^T/\varepsilon_0$ of 1,059 in poled BNKBMTx can be obtained around the MPB composition (because of the enhanced mobility of the domain and domain walls) with an obviously lower dielectric loss of 0.017 than the pure BNT–BT [22] and BNT–BKT [12] solutions.

Ferroelectric properties

Figure 5a–h shows the ferroelectric-hysteresis loops of BNKBMTx with the composition x of 0–0.28 under an electric field of about 4 kV/mm at 10 Hz. Typical hysteresis loops with rectangular shape can be observed for all the compositions. Similar to the dielectric constant, the remnant polarization P_r first increases from $\sim$26 to–29 μC/cm^2 with the x increasing (0–0.04) and then decreases to $\sim$7 μC/cm^2 with x further increasing (0.08–0.28). In comparison, the

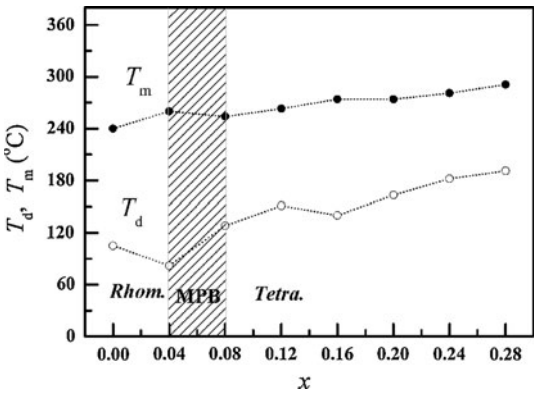

Fig. 3 Phase diagram for the proposed (Mn, K) modified BNT–BT solid solutions

coercive field E_c first decreases and then follows an increasing instead. Around the MPB composition x of 0.04, a maximum P_r of ~29 μC/cm^2 and minimum E_c of ~2 kV/mm can be obtained.

Besides, the temperature dependence of the *P-E* loops were also investigated for the composition x of 0.04 and 0.08 as shown in Fig. 6a and b. For the BNKBMT0.04, with the temperature increasing from room temperature to around 80 °C, weak double hysteresis loop can be detected and both the P_r and E_c decreases obviously. This temperature is consistent with ferroelectric to antiferroelectric phase transition temperature T_d obtained from the dielectric spectrum (Fig. 2b). With the temperature further increasing, the double hysteresis loops become much slimmer and both the P_r and E_c decrease greatly because of easier domain wall motion at elevated temperature. In comparison, the *P-E* loops of BNKBMT0.08 exhibits a similar temperature dependence behavior with a higher ferroelectric to antiferroelectric transition temperature of around 110 °C.

Piezoelectric properties

The bipolar *S-E* curves for the BNKBMTx ceramics with x of 0–0.12 were measured under an electric field of ~4 kV/mm at 10 Hz shown in Fig. 7. Around the MPB with x of 0.04, the maximum bipolar strain of ~0.25% can be obtained because of the enhanced-domain mobility. Figure 8 shows the piezoelectric constant d_{33} and normalized strain d^*_{33} ($= S_{max}/E_{max}$, obtained from the unipolar strain measured under an electric field of 4 kV/mm at 0.5 Hz) as a function of the concentration x. For the BNKBMTx ceramics, typical linear strain with little hysteresis can be obtained and it is evident from Fig. 8 that the maximum d_{33} and d^*_{33} for the MPB composition x of 0.04 can reach 155 pC/N and 290 pC/N, respectively. With the composition further increasing to 0.28, the d_{33} and d^*_{33} decreases instead. It need to be mentioned that larger d^*_{33} values than d_{33} should be correlated with different measuring frequencies as also observed in other BNT solution [12] and relaxor ferroelectric single-crystal $Pb(Mg_{1/3}Nb_{2/3})O_3$–$PbTiO_3$ [23]. Owing to the lower measuring frequency (d^*_{33}@0.2 Hz, d_{33} @55 Hz), the domain and domain walls possess enough time to follow external electric field and therefore larger piezoelectric constant can be obtained.

Compared to the Wang et al.'s results [24], this solid solution exhibits a higher d_{33} along with a lower dielectric loss tanδ as a result of the Mn ion doping. Besides, because of both the high-depolarization temperature up to 182 °C and relatively high d_{33} of 130 pC/N, the tetragonal BNKBMT0.24 ceramics would be also very promising for high-temperature solid state actuators and transducers.

Conclusions

In summary, the modification effect of Mn and K on the MPB composition $0.935Na_{0.5}Bi_{0.5}TiO_3$–$0.065BaTiO_3$ ceramics was systematically studied and piezoelectric, dielectric, ferroelectric properties along with the phase transition characteristics were characterized. The tolerance factor for the present solution with MPB composition was calculated to be 0.984–0.986 and coincided with the experience value of t_{MPB} (0.982–0.986) very well. A MPB region formed between the ferroelectric rhombohedral and tetragonal phases, where a

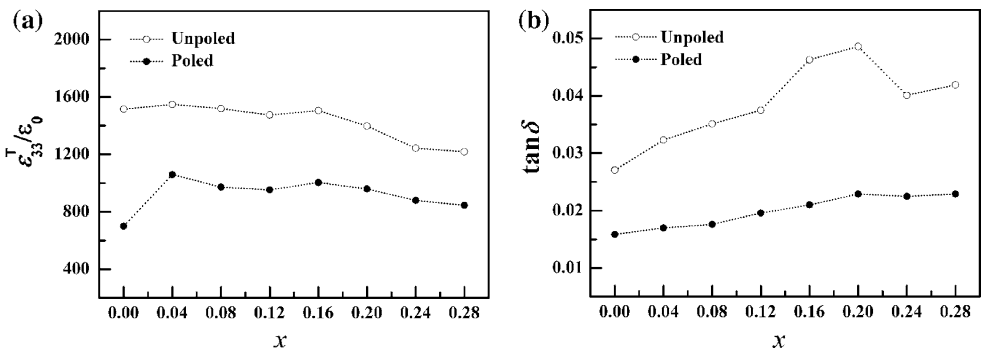

Fig. 4 Composition dependence of **a** the relative dielectric constant $\varepsilon^T_{33}/\varepsilon_0$ and **b** the dielectric loss tanδ before and after poled at 1 kHz

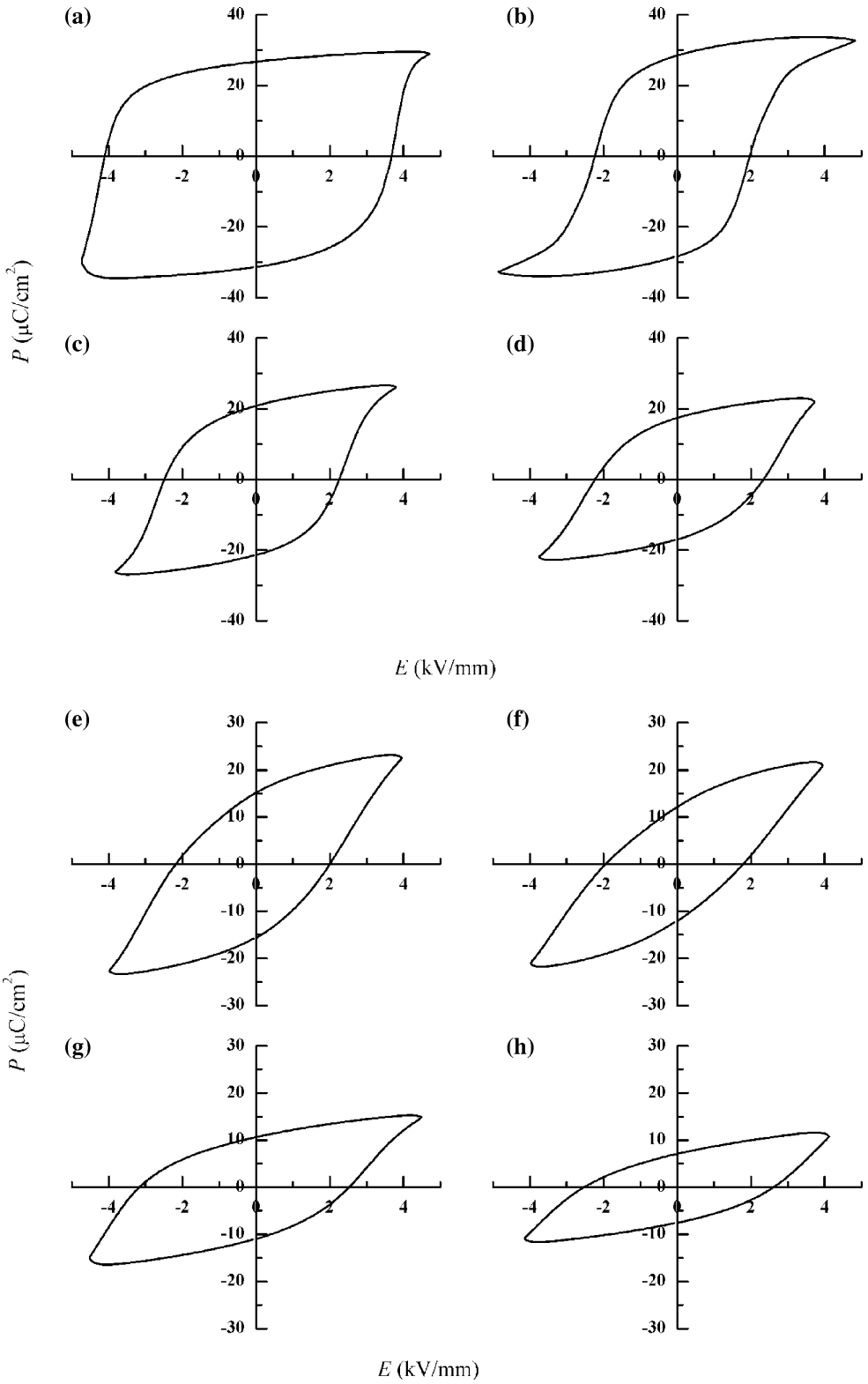

Fig. 5 The *P-E* loops of BNKBMT*x* with the composition *x*, **a** 0, **b** 0.04, **c** 0.08, **d** 0.12, **e** 0.16, **f** 0.20, **g** 0.24, and **h** 0.28, under an electric field of ~4 kV/mm at 10 Hz

maximum d_{33} of 155 pC/N, d_{33}^* of 290 pC/N, $\varepsilon_{33}^T/\varepsilon_0$ of 1,059 and low loss tangent tanδ of 0.017 were obtained. Besides, high-depolarization temperature of 182 °C was obtained for the tetragonal BNKBMT0.24 with a relative high d_{33} of 130 pC/N. These results would provide multiple choices for the room and high-temperature applications.

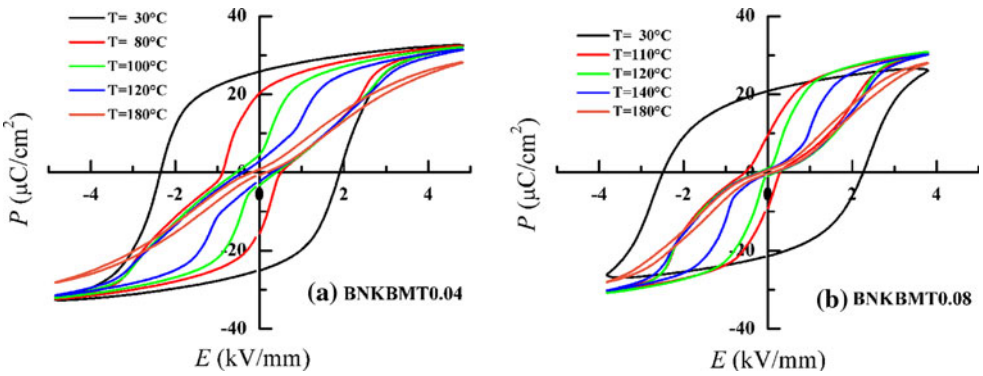

Fig. 6 The temperature dependence of the *P-E* curves for the composition *x* of **a** 0.04 and **b** 0.08 measured under an electric field of ~4 kV/mm at 10 Hz

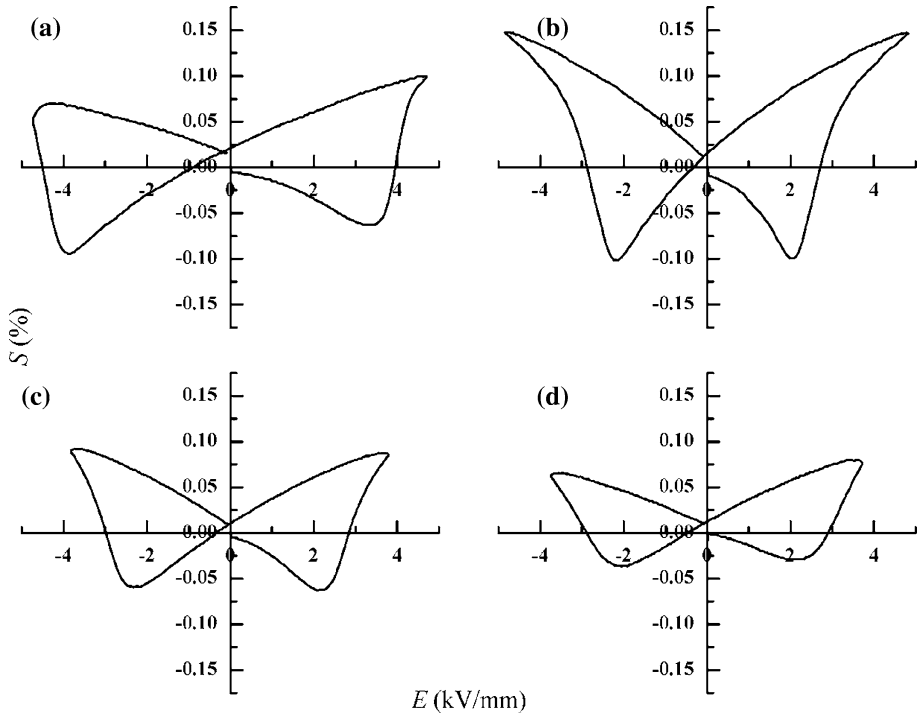

Fig. 7 The bipolar *S-E* curves for the BNKBMT*x* ceramics with *x* of **a** 0, **b** 0.04, **c** 0.08, **d** 0.12, measured under an electric field of about 4 kV/mm at 10 Hz

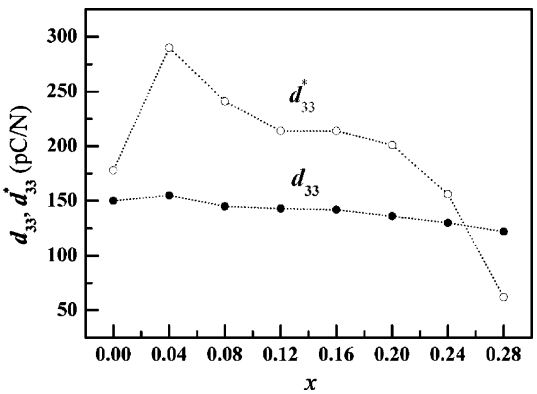

Fig. 8 The composition *x* dependence of the piezoelectric strain constant d_{33} and normalized strain d^*_{33} ($= S_{max}/E_{max}$, obtained from the unipolar strain measured under an electric field of ~4 kV/mm at 0.5 Hz)

Acknowledgement This study was supported by the Science and Technology Commission of Shanghai Municipality (Grant no. 10ZR1422300 and 09520501000), the Innovation Program of Shanghai Municipal Education Commission (Grant no. 11YZ82, 11YZ83, and 11ZZ117), Shanghai Normal University Program (SK201026 and PL929), National Natural Science Foundation of China (Grant no. 60807036), and Condensed Physics of Shanghai Normal University (Grant no. DZL712).

References

1. Jaffe B, Cook WR, Jaffe H (1971) Piezoelectric ceramics. Academic press, London
2. Directive 2002/95/EC of the European Parliament and of the Council of 27 January 2003, Official Journal of the European Union 2003, p L37/19
3. Maeder MD, Damjanovic D, Setter N (2004) J Electroceram 13:385

4. Rödel J, Jo W, Seifert TPK, Anton EM, Granzow T, Damjanovic D (2009) J Am Ceram Soc 92:1153
5. Eerd BW, Damjanovic D, Klein N, Setter N, Trodahl J (2010) Phys Rev B 82:104112
6. Hollenstein E, Davis M, Damjanovic D, Setter N (2005) Appl Phys Lett 87:182905
7. Trodahl HJ, Klein N, Damjanovic D, Setter N, Ludbrook B, Rytz D, Kuball M (2008) Appl Phys Lett 93:262901
8. Jones GO, Thomas PA (2002) Acta Crystallogr Sect B Struct Sci 58:168
9. Davis M, Klein N, Damjanovic D, Setter N, Gross A, Wesemann V, Vernay S, Rytz D (2007) Appl Phys Lett 90:062904
10. Smolenskii GA, Isupov VA, Agranovskaya AI, Krainik NN (1961) Sov Phys-Solid State Engl Transl 2:2651
11. Daniels JE, Jo W, Rödel J, Jones JL (2009) Appl Phys Lett 95:032904
12. Hiruma Y, Yoshii K, Nagata H, Takenaka T (2008) J Appl Phys 103:084121
13. Richard J, Pettry G, Said S, Marchet P, Mercurio JP (2004) J Eur Ceram Soc 24:1165
14. Liu WF, Ren XB (2009) Phys Rev Lett 103:257602
15. Lin DM, Zheng Q, Xu C, Kwok KW (2008) Appl Phys A Mater Sci Process 93:549
16. Shieh J, Wu KC, Chen CS (2007) Acta Mater 55:3081
17. Priya S, Kim HW, Ryu J, Zhang SJ, Shrout TR, Uchino K (2002) J Appl Phys 92:3923
18. Zhang QH, Zhang YY, Wang FF, Wang YJ et al (2009) Appl Phys Lett 95:102904
19. Hiruma Y, Nagata H, Takenaka T (2009) Appl Phys Lett 95:052903
20. Shannon RD (1976) Acta Crystallogr Sect A Cryst Phys Diffr Theor Gen Crystallogr A32:751
21. Smolenskii GA (1970) J Phys Soc Jpn 28:26
22. Shrout TR, Zhang SJ (2007) J Electroceram 19:113
23. Wang FF, Luo LH et al (2007) Appl Phys Lett 90:212903
24. Wang XX, Choy SH, Tang XG, Chan HLW (2005) J Appl Phys 97:104101